Quantitative Analysis of Single-Molecule RNA-Protein Interaction

Alexander Fuhrmann,[†‡] Jan C. Schoening,[§] Dario Anselmetti,[†] Dorothee Staiger,[§*] and Robert Ros[‡]
[†]Experimental Biophysics and Applied Nanoscience, Department of Physics, Bielefeld University, Bielefeld, Germany; [‡]Department of Physics, Arizona State University, Tempe Arizona; and [§]Molecular Cell Physiology, Department of Biology, Bielefeld University, Bielefeld, Germany

ABSTRACT RNA-binding proteins impact gene expression at the posttranscriptional level by interacting with cognate *cis* elements within the transcripts. Here, we apply dynamic single-molecule force spectroscopy to study the interaction of the *Arabidopsis* glycine-rich RNA-binding protein *At*GRP8 with its RNA target. A dwell-time-dependent analysis of the single-molecule data in combination with competition assays and site-directed mutagenesis of both the RNA target and the RNA-binding domain of the protein allowed us to distinguish and quantify two different binding modes. For dwell times <0.21 s an unspecific complex with a lifetime of 0.56 s is observed, whereas dwell times >0.33 s result in a specific interaction with a lifetime of 208 s. The corresponding reaction lengths are 0.28 nm for the unspecific and 0.55 nm for the specific *At*GRP8-RNA interactions, indicating formation of a tighter complex with increasing dwell time. These two binding modes cannot be dissected in ensemble experiments. Quantitative titration in RNA bandshift experiments yields an ensemble-averaged equilibrium constant of dissociation of $K_D = 2 \times 10^{-7}$ M. Assuming comparable on-rates for the specific and nonspecific binding modes allows us to estimate their free energies as $\Delta G^0 = -42$ kJ/mol and $\Delta G^0 = -28$ kJ/mol for the specific and nonspecific binding modes, respectively. Thus, we show that single-molecule force spectroscopy with a refined statistical analysis is a potent tool for the analysis of protein-RNA interactions without the drawback of ensemble averaging. This makes it possible to discriminate between different binding modes or sites and to analyze them quantitatively. We propose that this method could be applied to complex interactions of biomolecules in general, and be of particular interest for the investigation of multivalent binding reactions.

INTRODUCTION

Posttranscriptional regulation represents a key mechanism to control gene expression and includes pre-mRNA maturation, mRNA transport, translation, and breakdown (1). All these steps of RNA metabolism are accompanied by the activities of a suite of RNA-binding proteins in the cell. By interacting with *cis* elements within the transcribed portion of a gene they impact its expression pattern (2,3). To understand the molecular underpinnings of target site recognition is a prerequisite for understanding the functional implications of RNA binding (4).

We have characterized a family of small RNA-binding proteins with one terminal RNA recognition motif (RRM) and a C-terminal glycine-rich stretch in *Arabidopsis thaliana*. The prototypes *At*GRP7 (*A. thaliana* glycine-rich RNA-binding protein) and *At*GRP8 undergo circadian oscillations in transcript and protein abundance with peaks at the end of the daily light phase. Notably, *At*GRP7 and *At*GRP8 negatively autoregulate and crossregulate their expression through alternative splicing: interaction of the proteins with their own pre-mRNAs promotes the use of a cryptic intronic 5′ splice site, leading to incomplete intron removal and Nonsense-mediated decay of the alternatively spliced transcripts. *At*GRP7 also influences the steady-state abundance of other circadian regulated transcripts, suggesting that the *At*GRP7 feedback loop acts as a slave oscillator downstream of the circadian clock (5–7). Furthermore, *At*GRP7 and *At*GRP8 have been implicated in pathogen defense and in the transition to reproductive development by influencing the key floral repressor *FLC* (8,9). Thus, *At*GRP8, like *At*GRP7, presumably is an important posttranscriptional regulator in *Arabidopsis*.

To quantitatively investigate the *At*GRP8-RNA interaction with respect to binding specificity, apparent affinities, and associated timescales, we designed experiments at the single-molecule level. Interaction studies on biomolecules by classical ensemble experiments are often hindered by the fact that beyond the expected active constituents, molecular subpopulations with different binding properties can mask or broaden signals. Examples are molecules in a denatured, incorrectly folded, labile, or defective conformational state, or molecules that can adopt several metastable conformations. For regulatory molecules whose activity is often triggered by chemical modifications or structural changes, a subtle analysis of interaction data is mandatory for identification and quantification of the key binding mechanisms (10). The advent of single-molecule technologies has fostered new biophysical approaches to detect and quantify molecular interaction on various systems (11). In particular, single-molecule force spectroscopy (SMFS), based on atomic force microscopy (AFM) (12), has proven to be an appropriate tool to investigate ligand-receptor interactions with a sensitivity of single-point mutations in an affinity range (K_D) of 10^{-4}–10^{-15} M, providing access to molecular forces, elasticities, reaction off-rate constants, and binding-energy landscapes without being subject to avidity and

Submitted August 13, 2008, and accepted for publication March 11, 2009.

Alexander Fuhrmann and Jan C. Schoening contributed equally to this work.

*Correspondence: dorothee.staiger@uni-bielefeld.de

Editor: Taekjip Ha.

0006-3495/09/06/5030/10 $2.00

doi: 10.1016/j.bpj.2009.03.022

rebinding phenomena (10,11,13–25). Over the last years, a number of pioneering attempts have been published to characterize intra- and intermolecular RNA interactions in single-molecule experiments. By single-molecule AFM imaging, Henn et al. analyzed the unwinding properties of duplex RNA by the DbpA protein (26) and Bonin et al. investigated the specific binding of the iron responsive element binding protein to the iron responsive element presented within a dsRNA backbone (27). Klaue et al. investigated the binding of the RNA editing enzyme ADAR2 to large dsRNA-fragments in AFM imaging experiments and resolved individual complexes that allowed structural differentiation between editing and nonproductive binding sites (28). Cho et al. investigated the complexation of the HIV transactivation response element with TAT-derived peptides in chemical force microscopy and force spectroscopy experiments. They found a pH-dependent binding-related chemical contrast on microstructured surfaces, but without single-molecule resolution (29). Recently, Vilfan et al. published biochemical toolbox strategies to control, interface, and assemble RNA constructs for SMFS experiments (30).

Here, we present the first single-molecule AFM-SMFS investigation that we know of that quantitatively interprets the interaction between an individual RNA binding protein (RBP) and its RNA target along an advanced theoretical framework of single-molecule binding, allowing insights into different binding modes and their associated binding-energy landscapes.

The appropriate analysis of the respective data is commonly based on the pioneering work presented by Evans and Ritchie in their standard theory (31). This was recently modified and extended within the theoretical framework of a heterogeneous bond model (32). Furthermore, a refined data analysis technique allows the discrimination of different possible subpopulations and gives insights into the associated molecular binding modes and mechanisms (33). Since the interaction of *At*GRP8 with its target sequence is expected to be rather complex and to depend on the secondary structure of the RNA target, we applied this refined analysis procedure for a detailed and quantitative characterization of this interaction at the single-molecule level.

MATERIALS AND METHODS

RNA bandshift assays

The following synthetic oligoribonucleotides (ORNs) were purchased from Biomers (Ulm, Germany):

8-UTR_WT GUUUUUGGUUUAGAUUUGGUUUUGUGU
8-UTR_WT-SH GUUUUUGGUUUAGAUUUGGUUUUGUGU C_3-SH
8-UTR_G_6mut GUUUUUAAUUUAAAUUUAAUUUUAUGU C_3-SH.

The ORNs were 5′-labeled with γ-[^{32}P] ATP as described (34). Recombinant GST fusion proteins were purified from *Escherichia coli* by chromatography on glutathione sepharose (35).

The binding assays contained 50 fmol of labeled oligonucleotide, 0.5 μg recombinant GST-*At*GRP8, 20 mM HEPES-KOH, pH 7.5, 100 mM NaCl, 1 mM $MgCl_2$, 0.01% NP-40, 10 U RNAsin, tRNA, and unlabeled competitor as indicated. Incubation was performed for 20 min at room temperature. The binding reactions were resolved on 6% polyacrylamide gels in 40 mM Tris-acetate, 1.8 mM EDTA. The gels were dried and analyzed using a Typhoon 8000 phosphorimager and ImageQuant software (GE Healthcare, Freiburg, Germany).

For determination of equilibrium dissociation constants (K_d), increasing amounts of protein were incubated with 50 fmol of labeled oligonucleotide. The amount of radioactivity in the retarded complex and the free ORN were quantified using Image Quant Software. The log (complexed/free probe) was plotted against the log (protein concentration). Lines were obtained by linear regression based on the mean of three independent experiments. The log (K_d) is obtained as the x-intercept (5,7).

Sample surface and AFM tip modification

For AFM-SMFS measurements, sample surfaces and AFM tips were functionalized as described previously (10,13,20,22). Briefly, Si_3N_4 cantilevers (MSCTAU-HW, Veeco Instruments, Santa Barbara, CA) were activated by dipping for 3 s in concentrated nitric acid and silanized in a solution of 2% aminopropyltriethoxysilane in dry toluene for 2 h. After heating the RNA at 80°C for 5 min, the 2 mM RNA was mixed with 2 mM *N*-hydroxysuccinimidepoly(ethylene glycol)-maleimide (Nektar, Huntsville, AL) and then stored at 4°C overnight. The cantilevers were subsequently incubated in the RNA-PEG solution for 2 h and extensively washed with binding buffer (25 mM HEPES-KOH, pH 7.5, 150 mM NaCl, 2 mM $MgCl_2$, 0.1% NP-40) before use.

Mica surfaces (Provac AG, Balzers, Liechtenstein) were silanized with aminopropyltriethoxysilane in a desiccator and incubated with 50 μM bis (sulfosuccinimidyl) suberate-sodium salt and 50 μM *At*GRP8 fusion protein. After 1–2 h, the surface was washed with binding buffer. The modified surfaces were stable for at least 1 day if stored at 4°C.

Dynamic force spectroscopy and data analyis

Force spectroscopy measurements were performed with a commercial AFM (MFP-3D, Asylum Research, CA) at 24°C. All raw data force curves were filtered by the default cut-off frequency low-pass filter in the MFP-3D software. The spring constants of all AFM cantilevers were calibrated by the thermal fluctuation method (36) included in the MFP-3D software and were typically in a range from 15 to 18 pN/nm. In dynamic force spectroscopy (DFS), loading-rate-dependent measurements were performed, where the retraction velocity of the piezo was varied while the approach velocity was kept constant at 5 μm/s. The time during which the AFM tip is in contact with the surface is called dwell time. This time can be set in the software of the AFM. However, the built-in software starts this dwell time after a certain trigger point is reached (always set to 800 pN). This causes slight deviations from the real contact time. To account for that problem, the dwell time was calculated here as the total time span where the tip contacted the sample during the approach the first time until it left the sample during retraction. The measured individual force-distance curves were analyzed with a MATLAB program (The MathWorks, Natick, MA) in an automated manner (33). In this study, the binning sizes for the force and rigidity values were set to 20 pN and 0.75 pN/nm, respectively. The histograms, and thus the height color bars, have been normalized to the total number of force distance curves taken. Data analysis was done by an enhanced method, described in our previous work (33), using a home-built software written in C-programming language. The maximum likelihood estimates to gather the quantitative parameters are done by a commercial algorithm (NAG library).

RESULTS

*At*GRP8 interacts with its own mRNA

To investigate an interaction of the *At*GRP8 protein with its own mRNA at the single-molecule level, we used a synthetic

ORN derived from the *At*GRP8 3′ untranslated region as the binding substrate, which has been shown to be a binding site for *At*GRP7 (5). The 27mer ORN carried a thiol group at its 3′ terminus (8-UTR_WT-SH). Conventional RNA bandshift assays confirmed that the interaction of the thiol-terminated radiolabeled ORN with recombinant *At*GRP8 was indistinguishable from that of the unmodified 8-UTR_WT ORN (Fig. S1 in the Supporting Material). Thus, the thiol tag does not interfere with complex formation. The ORN was covalently attached to silicon nitride AFM tips via a 30-nm poly(ethyleneglycol) spacer. Recombinant glutathion S-transferase (GST)-*At*GRP8 fusion proteins were functionally attached in low densities to mica surfaces using standard covalent chemistry. In AFM-SMFS experiments, the RNA-functionalized AFM tip is moved toward and then retracted (cycled) from the protein-covered surface with simultaneous recording of the forces acting on the AFM-cantilever (Fig. 1 *A*). In these force-distance curves, individual binding events can be identified as force discontinuities in the retracting force-distance trace between the point of dissociation and the force baseline (Fig. 1 *B*), as described in detail (33). A nonlinear part of the force-distance curve precedes the abrupt dissociation event. Although the physical model that best describes the force-extension characteristic is the freely jointed chain model (37,38), it would still be unknown how to describe protein-RNA extension in the bound stage. Since we only need to know the force acting on the molecule bond as a function of time for our further quantitative data analysis, we decided to simply fit a polynomial second grade into our data. This fit describes the force-extension characteristics in the relevant interval very well (*red line*). The slope of this polynomial at the point of dissociation is called ''rigidity'' and describes the total elasticity of the cantilever, spacers, and molecular complex at the point of rupture. The dissociation events are stochastic in nature, obeying the law of a thermally activated decay of a metastable state, and have to be analyzed in a statistical way (31–33). This implies that all curves with the same constant velocity of pulling must follow the same path before the complex dissociates, and only the point of rupture differs due to the statistical process. For the analysis undertaken later (see below), this path has also to be independent from the pulling velocity (32,33,39,40).

Upon plotting the data of all observed dissociation events (dissociation forces and rigidity) for a particular retraction velocity (here, 5000 nm/s) in a 2D force-rigidity histogram plot (Fig. 1 *C*), the following observations can be made. First, a projection of the 2D histogram onto a 1D probability-force histogram is generated. This standard force histogram plot (number of rupture events over dissociation force) exhibits a rather broad force distribution, which cannot be adequately modeled along the standard model of dissociation under external force.

Second, the 2D-histogram plot shows a nonuniform distribution with distinct peaks. A model with one distinct dissociation mode for the observed complex (with particular kinetic parameters and equilibrium constants) would result in a unimodal distribution in this plot. There are two likely explanations for the presence of multiple peaks: there could be multiple force-extension characteristics, or all of these curves could follow the same path before the complex dissociates (with the exception that for one pulling velocity, the

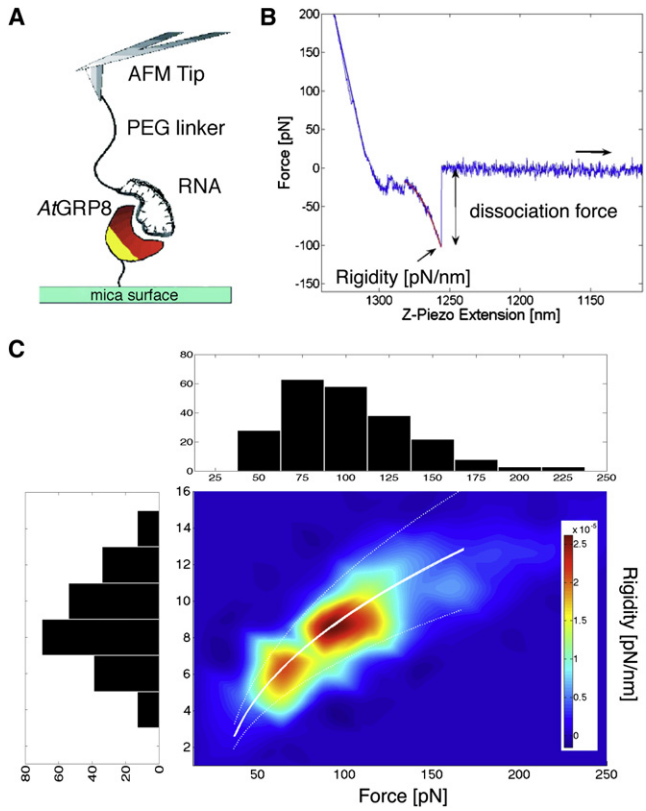

FIGURE 1 (*A*) Schematic illustration of an SMFS experiment. Recombinant RNA binding protein (GST-*At*GRP8) is covalently immobilized on a mica surface. The corresponding synthetic RNA oligonucleotide is connected via a poly(ethylene glycol) linker to the tip of a silicon nitride AFM cantilever. The distance between surface and tip can be controlled with a piezoelectric element while the force acting between the tip and surface is detected. (*B*) A typical force-distance curve (only the retracting part of the complete force-distance cycle is shown). The nonlinear part of the force-distance curve that precedes the abrupt dissociation event can be fitted by a second-degree polynomial (*red line*). The slope of this polynomial at the point of dissociation is called rigidity and the corresponding force difference between the point of dissociation and the force baseline is defined as the dissociation force. (*C*) Data from individual dissociation events (dissociation force, rigidity) of the investigated RNA-protein interaction at a pulling velocity of 5000 nm/s are plotted in a 2D probability histogram (*red*, high frequency; *blue*, low frequency), in which only events with a force-extension characteristic similar to the constructed master curve are taken into account (for details, see Fuhrmann et al. (33)). Projections of the cumulative distributions of the dissociation force and the rigidity are shown as additional 1D graphs above and to the left of the 2D histogram. The white line indicates the corresponding values of rigidity force for the master curve and the dashed white lines flanking the master curve correspond to the maximum allowed deviation of the rigidity. The color scale represents the rupture frequency, normalized to the total number of acquired force-distance curves and number of binning fields.

point of rupture differs due to the statistical process). By introducing a master curve and comparing the single force-distance curves to this master curve, the latter explanation was confirmed: all peaks can be explained by one single master curve (which includes all of the pulling velocities). For details, see the Data analysis section and our previous work (33). For visual support, the corresponding values of the master curve (rigidity = slope at certain force) have been plotted as a solid white line in Fig. 1 *C*. The dashed white lines flanking the master curve correspond to the maximally allowed deviation of the rigidity. It is important to restrict the data to single-molecule events. Therefore, a low surface density of the immobilized proteins was utilized. AFM images of the surfaces show densities of ~20–30 molecules/μm^2 (data not shown). As a result, the overall probability of observing a rupture event in the retracting force-distance trace is <30%. Higher protein surface densities increase the binding probability but also yield a drastically increased number of multiple interactions. Furthermore, the poly(ethyleneglycol) spacer dramatically reduces the amount of muticomplex ruptures, as well as the forces due to direct tip-surface interactions (16,18). Because of the small radius of the AFM tip and the small length distribution of the spacer, MALDI measurements indicate a variance of 30 ± 5 nm for the molecules used, the rupture of multiple complexes can be distinguished by a sawtooth pattern in the force-distance before the rupture. Only events with ruptures between 30 and 47 nm are taken into account.

Third, if we fit a freely jointed chain model (38) into our data (more precisely into the constructed master curve (see below)), we obtain a Kuhn length of 0.54 nm, consistent with findings from mechanical experiments on single poly (ethyleneglycol) molecules.

To assess the specificity of the observed interaction between *At*GRP8 and 8-UTR_WT-SH, the following control experiments were carried out: First, we investigated a potential influence of the GST moiety on the observed binding. The respective distribution for the SMFS experiment with immobilized GST protein and 8-UTR_WT-SH ORN exhibited no significant interaction or binding probability (data not shown). This indicates a negligible unspecific background due to interactions between the RNA on the tip and the surface. The probability of observing a binding event is 1% for the slower-retracting velocity of 500 nm/s and <1% for 5000 nm/s, compared to 25% for 500 nm/s and 29% for 5000 nm/s between GST-*At*GRP8 and 8-UTR_WT-SH, respectively (Fig. 2, *A* and *B*). It is worth noting that all control experiments were conducted at two different retracting velocities (500 nm/s and 5000 nm/s) to check for possible dynamic phenomena. The corresponding graphs (compare images at left (500 nm/s) with those at right (5000 nm/s)) reveal a shift toward larger interaction forces with experimental velocity, in full agreement with theory (31–33).

Next, we probed the binding between *At*GRP8 and a mutant RNA sequence with six guanine residues of the authentic binding site exchanged for adenine (8-UTR_G_6mut-SH) (Fig. 2, *C* and *D*). RNA bandshift assays showed that mutation of these G residues largely abolished the ability to compete for complex formation with 8-UTR_WT-SH ORN (Fig. S2). We found reduced binding probabilities of 20% and 1% for the 500 nm/s and the 5000 nm/s data, respectively. Further control experiments with a 27mer poly(A) ORN as binding substrate also resulted in a nearly complete suppression of binding events (1% for 500 nm/s and 1% for 5000 nm/s; data not shown).

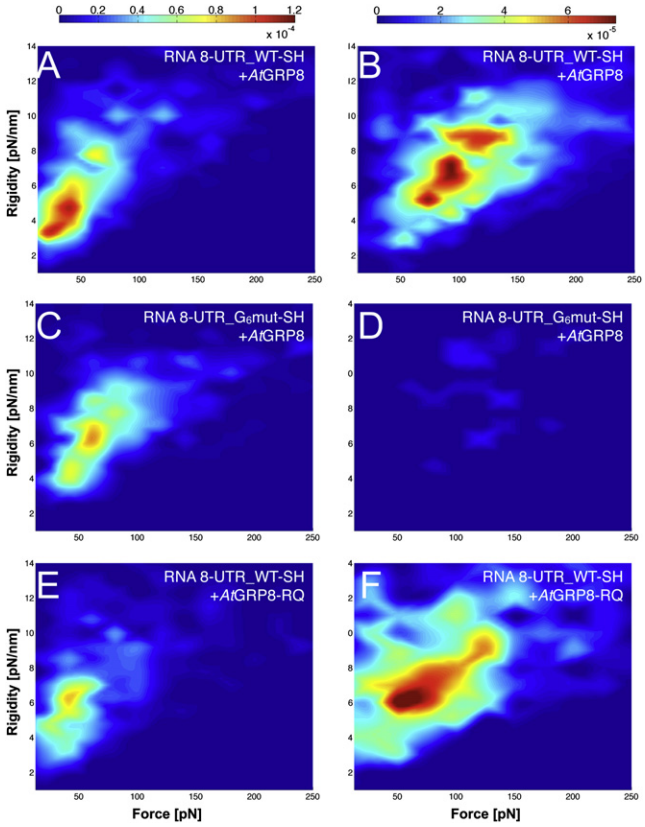

FIGURE 2 Normalized 2D probability histograms including all measured rupture force events without master curve filtering for two different experimental speeds, v = 500 nm/s (*left column*) and v = 5000 nm/s (*right column*). (*A* and *B*) 8-UTR_WT-SH ORN versus *At*GRP8. (*C* and *D*) mutant RNA (8-UTR_G_6mut-SH) versus *At*GRP8. (*E* and *F*) 8-UTR_WT-SH ORN versus mutant *At*GRP8-RQ. The color scales represent the normalized rupture frequencies for *A*, *C*, and *E* (*left*) and *B*, *D*, and *F* (*right*).

Finally, we used a mutant version of the *At*GRP8 fusion protein, *At*GRP8-RQ, with the conserved arginine residue at the beginning of RNP1 exchanged for glutamine (7). An analogous mutation within *At*GRP7 had been shown to reduce binding affinity about sixfold in RNA bandshift assays without impairing protein folding (5). As a consequence, the 2D histograms for the higher velocity (Fig. 2, *E* and *F*) changed and the center of gravity of the observed dissociation events clearly shifted to smaller forces compared to the wild-type protein (Fig. 2 *B*). As shown below, this behavior is compatible with a pro rata reduction

in specific interaction and an equivalent increase in unspecific interaction.

Dwell-time-dependent lifetimes and molecular parameters

*At*GRP8 and its RNA target display rather complex binding characteristics, as can be seen in the 1D force histogram by their correspondingly broad force distribution, which splits into two peaks in the novel 2D histogram representation (Fig. 1 *C*). To explain the apparent subpopulations, we varied the dwell time, during which the AFM tip is in contact with the surface.

A detailed analysis of the experimental dissociation events between *At*GRP8 and 8-UTR_WT-SH ORN on dwell time yielded a clear and significant dependence of the identified subpopulations on dwell time. In Fig. 3, the corresponding 2D histograms are shown for dwell times of $\tau_1 = 0.10$–0.21 s (Fig. 3 *A*), $\tau_2 = 0.22$–0.32 s (Fig. 3 *B*), and $\tau_3 = 0.33$–0.60 s (Fig. 3 *C*), all taken at an experimental retraction velocity of 5000 nm/s. It is clear that a transformation from a population with small dissociation forces for the short dwell time, τ_1, to a population with larger dissociation forces for τ_3 can be discerned. The medium dwell time, τ_2, shows an overlay of the distributions from τ_1 and τ_3, indicating that both subpopulations are populated. Another explanation for high rupture forces might be an increased amount of multiple rupture events. However, the rupture force distribution at long dwell times is very narrow, which would be very unlikely in case of multiple rupture events. Also, for dwell times from 0.35 s to 1 s, the force distribution remains unchanged (data not shown). To verify that the dwell time does not influence our principle SMFS setup, we reanalyzed data from previous experiments (33). In those experiments, we measured the interaction of recombinant protein applied to the surface with DNA attached at the tip via the same linker used for RNA in this work. We could not detect any influence of the dwell time on the rupture forces except for a slightly higher rupture probability.

This is compatible with the hypothesis that the more time the complex has to arrange (and therefore the dissociation force increases), the higher the probability of finding a tighter interaction. To prove this hypothesis, we statistically analyzed all the measured dissociation events within the theoretical framework of our extended and recently published DFS theory, wherein local bond parameters are allowed to fluctuate within a certain degree (32,33). According to the standard and extended theory for SMFS (31–33), a thorough statistical analysis allows extraction and estimation of thermal reaction off-rate constants (k_{off}) and reaction lengths that go beyond the determination of molecular interaction forces. Describing the dissociation of a complex due to the application of a constant external force can be done within the framework of classical reaction rate theory (31,41). In the Bell model, the externally applied force lowers the potential

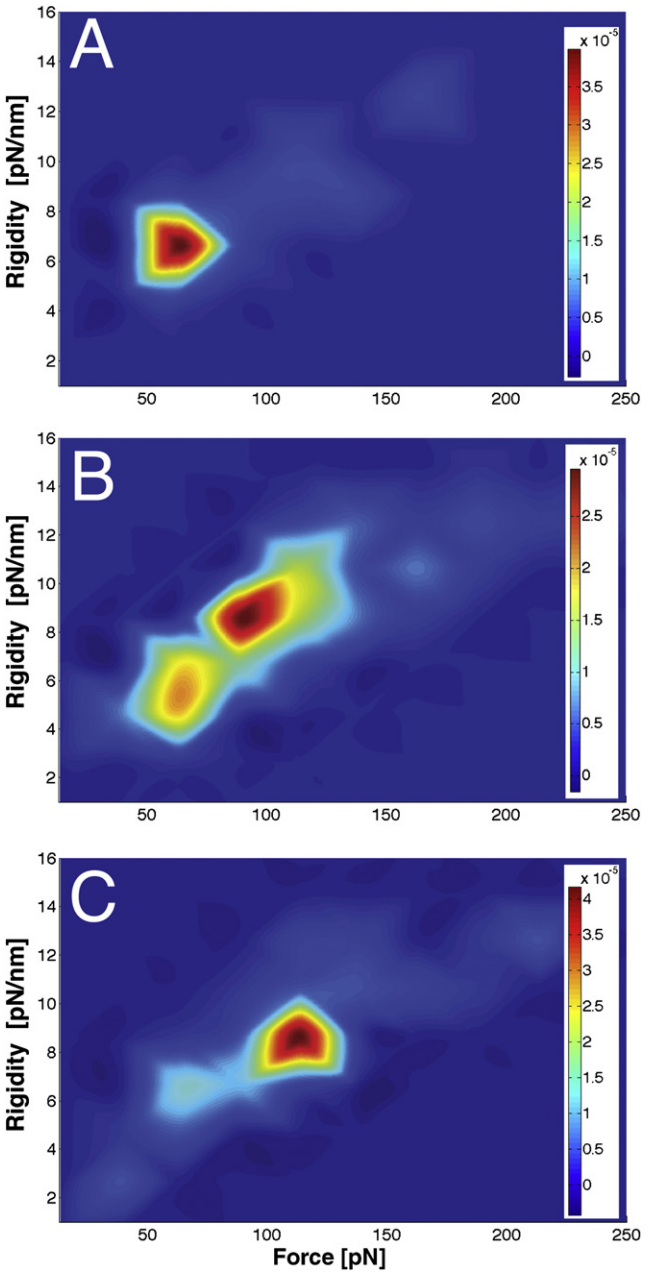

FIGURE 3 Dwell-time-dependent 2D histograms of 8-UTR_WT-SH ORN-*At*GRP8 interaction measured at an experimental velocity of 5000 nm/s (same data as in Fig. 1 *C*) for (*A*) dwell times of 0.10–0.21 s, (*B*) dwell times of 0.22–0.32 s, and (*C*) dwell times of 0.33–0.60 s. Representative plots of three independent repetitions are displayed. The color scale indicates the normalized rupture frequency.

barrier, whereas the barrier width (also known as reaction length) x_β, i.e., the difference between the maximum of the potential barrier and the minimum of the metastable state along the reaction coordinate, remains constant. This yields to the Bell rate (41):

$$k_{off}(f) = k_{off}^0 \exp\left(\frac{f x_\beta}{k_B T}\right), \quad (1)$$

where f is the most probable dissociation force, k_{off}^0 the rate of dissociation at zero applied force, T the temperature, and k_B the Boltzmann constant.

Since the changes of the acting force on the bond molecules are rather slow in comparison to molecular relaxation processes, the reaction kinetics can be approximated by

$$\frac{dp(t)}{dt} = -k_{off}(f(t))p(t), \tag{2}$$

where $p(t)$ denotes the survival probability of the bond at a given time, t.

Assuming that the force as function of time, $f(t)$, depends solely on the total extension, $s = vt$, of all elastic components (molecules, linker, cantilever, etc.) leads to

$$F(s) = F(v \times t) = f(t), \tag{3}$$

where $F(s)$ is independent of the retraction velocity, v.

With Eq. 2, the formal solution of the survival probability of the bond under an externally applied force f for any $k_{off}(f)$ and $F(s)$ is given by Raible et al. (32).

$$p_v(f) = \exp\left\{ -\frac{1}{v}\int_{f_{min}}^{f} df' \frac{k_{off}\left(f'\right)}{F'\left(F^{-1}\left(f'\right)\right)} \right\}, \tag{4}$$

where $p_v(f(t)) = p(t)$ and $p(t = 0) = p_v(f_m = f_{in}) = 1$. Here, f_{min} is the threshold value below which dissociation forces cannot be distinguished from thermal fluctuations. In addition, it is assumed that the acting force increases strictly monotonically, so that the inverse function F^{-1} of $F(s)$ exists.

Starting from the survival probability of the bonds $p_v(f)$ at pulling velocity v (Eq. 4), a function $g(f)$ can be defined as

$$g(f) = -v \ln p_v(f). \tag{5}$$

Under the assumptions defined by Eqs. 2 and 3, this $g(f)$ should be independent of the pulling velocity. An estimate of $g(f)$ from the experimental data can be done in the following way (33). With a given data set consisting of N_v rupture forces, f_n ($n = 1, \ldots, N_v; f_n > f_{min}$ for all n) measured at a given retraction velocity, v, the true probability of bond survival, $p_v(f)$, can be estimated as

$$p_v(f) = \frac{1}{N_v}\sum_{n=1}^{N_v} \Theta(f_n - f), \tag{6}$$

where $\Theta(x) = \int_{-\infty}^{x} \delta(y)dy$ is the Heaviside step function $[\Theta(x < 0) = 0, \Theta(x > 0) = 1]$.

Using this, one can plot Eq. 5 as done in Fig. 4. It is obvious that there is a clear dependence on the pulling velocity (compare with Raible et al. (40)).

Raible et al. (32) introduced a new theoretical ansatz called heterogeneity of chemical bonds. The central element and solution of this heterogeneous bond model theory is that due to statistical and uncontrollable variations of the molecular complex, or of the local environment of the bond, the parameter x_β (reaction length) itself is subjected to random variations. This parameter is sampled from a Gaussian distribution with mean x_β and variance ${\sigma_x}^2$. The heterogeneous bond model thus involves the three parameters x_β, σ_x, and k_{off}.

Since these three variables change with every single experiment (i.e., each rupture event), only the averaged survival probability can be obtained:

$$\overline{p}_v(f;\vec{\mu}) = \frac{\int d\vec{\lambda}\, p(\vec{\lambda};\vec{\mu}) p_v(f;\vec{\lambda})}{\int d\vec{\lambda}\, p(\vec{\lambda};\vec{\mu}) p_v(f_{min};\vec{\lambda}),} \tag{7}$$

with $\vec{\lambda} = (k_{off}^0, x_\beta)$ and $\vec{\mu} = (k_{off}^0, x_\beta, \sigma_x)$.

For N independent experiments, the probability of measuring a set of rupture forces $\{f\}$ is the product of the single probabilities

$$P(\{f_i\};\vec{\mu}) = \prod_{i=1}^{N} P(f_i;\vec{\mu}). \tag{8}$$

By maximizing this function of $\vec{\mu}$ by a maximum likelihood estimate, the most probable values for x_β, σ_x, and k_{off} can be found in our previous work (33).

A requirement for this is to have a sufficient number of rupture events. To do so, typically thousands of force curves have to be evaluated, categorized, and quantified to yield accurate and reliable statistical numbers (33). This approach relies on a careful determination of the measured force distributions for various retraction velocities and is termed DFS.

When the experimental data are compared with the estimated parameters by plotting the function (Eq. 5) and the measured survival probabilities (Eq. 6), the results are in good agreement with the analyzed data sets (Fig. 4). The $-v\ln(p_v(f))$ versus f diagrams were plotted for the measured dissociation events between *At*GRP8 and 8-UTR_WT-SH ORN for the shortest (Fig. 4 *A*), medium (Fig. 4 *B*), and longest dwell times (Fig. 4 *C*).

The associated values for the modeled parameters can be found in Table 1. From this table it is evident that the lifetime, τ_{bond}, of the RBP-RNA complex and its reaction length x_β, which can be interpreted as the depth of the receptor binding pocket, strongly depend on the probed subpopulation. Namely, the distributions related to τ_1 and τ_3 of the *At*GRP8-8-UTR_WT-SH ORN complex yield lifetimes, τ_{bond}, of 0.56 s and 208 s and reaction lengths x_β of 0.28 nm and 0.55 nm, respectively, and can therefore be characterized with respect to the tightness and nesting of the bound complex. The distributions are related to the medium dwell time, τ_2, which shows that the characteristics of both subpopulations can be quantified to $\tau_{bond} = 92$ s and $x_\beta = 0.50$ nm. These values are very similar to the lifetime and reaction length of the total data set, $\tau_{bond} = 36$ s and $x_\beta = 0.51$ nm,

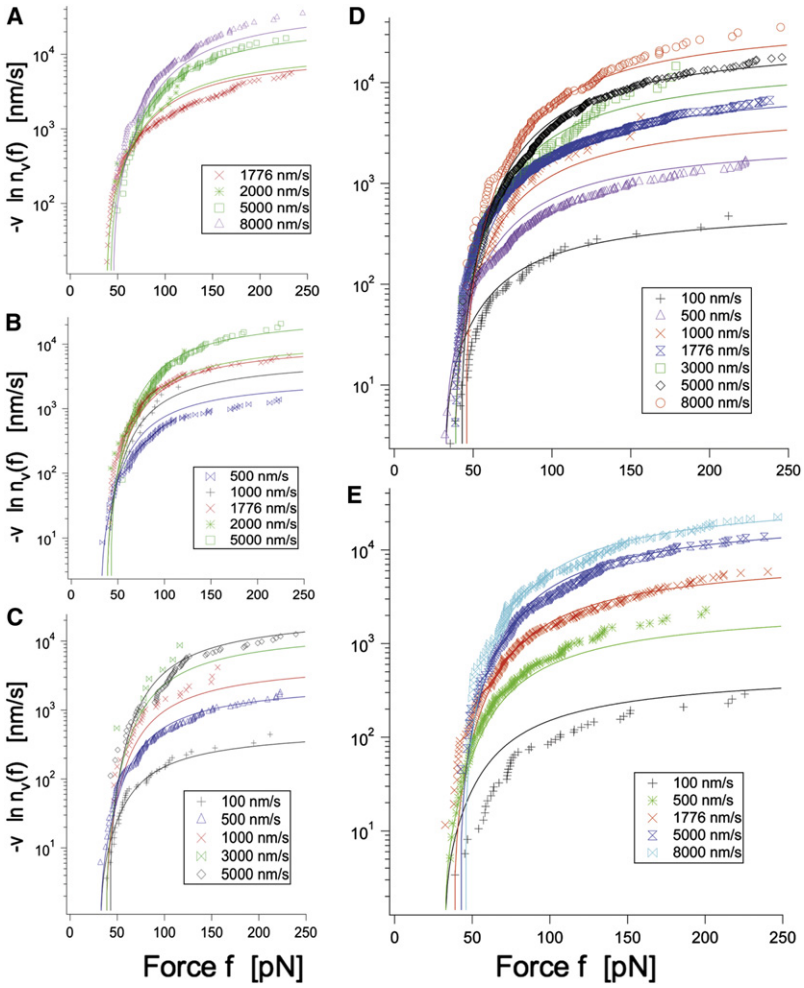

FIGURE 4 Dwell-time-dependent DFS analysis of 8-UTR_WT-SH ORN. RNA-*At*GRP8 interaction. The theoretical function $-v\ln(n_v(f))$ is fitted to the experimental data sets and plotted for all available retraction velocities. Only events with a force-extension characteristic similar to the constructed master curve $F(s)$ have been taken into account. Diagrams are shown for (*A*) all available dissociation datasets; (*B*) only dissociation events of the subpopulation with short dwell time, τ_1; (*C*) only dissociation events of the subpopulation with medium dwell time, τ_2; (*D*) only dissociation events of subpopulation with long dwell time, τ_3; and (*E*) all available dissociation datasets of the interaction of 8-UTR_WT-SH ORN with *At*GRP8-RQ. For details, see text.

which includes all experimental dwell times from 0.1 to 0.6 s (Fig. 4 *D*) and supports the hypothesis of two different binding modes. It is worth noting that only averaged values can be accessed in conventional ensemble experiments, because such experiments cannot discriminate between different subpopulations.

To gain insight into the specific binding mode, we measured the dissociation events between the *At*GRP8-RQ protein, which is mutated in a highly conserved Arg within the RNA recognition motif and the 8-UTR_WT-SH ORN at dwell times $\tau_4 = 0.4$–0.6 s (Fig. 4 *E*). This resulted in a clearly enhanced k_{off} and, hence, a much shorter lifetime, τ_{bond} (Table 1).

Competition of the *At*GRP8-RNA interaction in single-molecule experiments

In ensemble measurements by RNA bandshifts, binding specificity is assessed in competition experiments where an excess of unlabeled ORN is tested for its ability to compete with labeled ORN for the cognate binding protein (5,42). We set out to develop a similar competition experiment in SMFS experiments with native surface-functionalized *At*GRP8

TABLE 1 Properties of *At*GRP8-RNA interactions

RNA	Protein	Dwell time	k_{off} (s^{-1})	$\Delta\ln(k_{off})$	τ_{bond} (s)	x_β (nm)	Δx_β (nm)
RNA 8-UTR_WT-SH	*At*GRP8	τ_3	0.0048	1.8	208	0.55	0.10
RNA 8-UTR_WT-SH	*At*GRP8	τ_2	0.01	1.7	92	0.50	0.09
RNA 8-UTR_WT-SH	*At*GRP8	τ_1	1.8	6.3	0.56	0.28	0.03
RNA 8-UTR_WT-SH	*At*GRP8	τ_1–τ_3	0.027	0.6	36	0.51	0.03
RNA 8-UTR_WT-SH	*At*GRP8-RQ	τ_4	0.075	0.9	13.3	0.40	0.05

Off-rate constants (k_{off}), lifetimes of the complexes (τ_{bond}), and reaction lengths (x_β) are determined in accordance with a previous study (33). Dwell-time intervals were τ_1, 0.10–0.21 s; τ_2, 0.22–0.32 s; τ_3, 0.33–0.60 s; and τ_4, 0.40–0.60 s. Δx_β represents the statistical error of x_β, i.e., the standard deviation of the estimate of this quantity when the experiment is repeated many times.

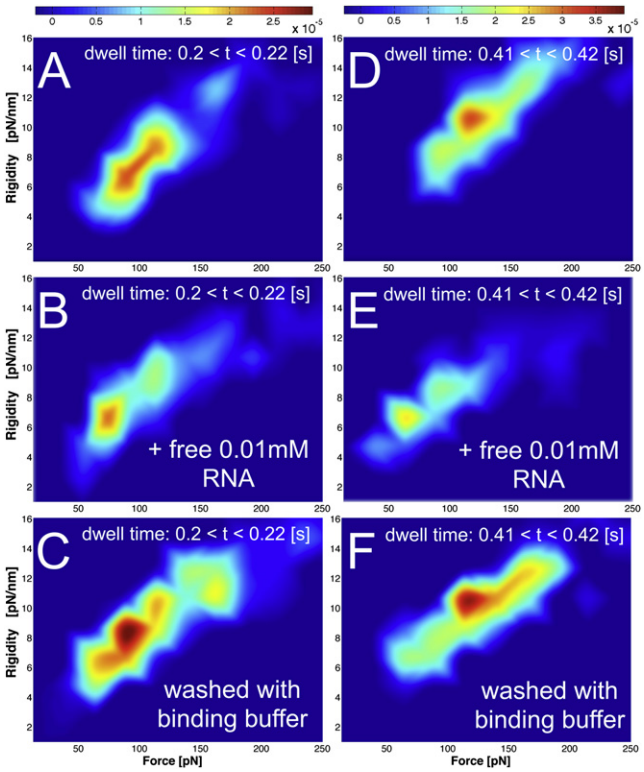

FIGURE 5 Dwell-time-dependent competition experiments between 8-UTR_WT-SH ORN and *At*GRP8 at 5000 nm/s. The 2D histograms for two different dwell times of 0.2–0.22 s and 0.41–0.42 s are normalized to the rupture probability and exhibit the different binding specificity of the subpopulations. For details, see text. The color scales represent the normalized rupture frequencies for *A–C* (*left*) and *D–F* (*right*).

protein and 8-UTR_WT-SH ORN. After the known activation profile had been verified in the 2D histogram for the two different dwell-time intervals, 0.20–0.22 s and 0.41–0.42 s (Fig. 5, *A* and *D*), free 8-UTR_WT ORN was added to the binding buffer at a concentration of 10 μM. Free 8-UTR_WT ORN, which can bind to the surface of the immobilized *At*GRP8 protein without temporal restrictions, theoretically blocks and inactivates the surface in a competitive manner for the functionalized AFM-tip. This experiment was conducted with an experimental retraction velocity of 5000 nm/s and the results were plotted in 2D histograms (Fig. 5, *B* and *E*).

It is worth noting that both dwell-time-dependent competition experiments yielded very similar results: the expected blocking affected mainly the subpopulation that is characterized by the longest lifetime, the largest reaction length, and dissociation force, which in addition turned out to be also the most specific one. The other subpopulation was practically not affected by the competing ORN, suggesting a rather unspecific interaction. Consecutively, the activity of the two surfaces could be reestablished by extensive washing with binding buffer, which removes the free RNA oligomers from the solution (Fig. 5, *C* and *F*).

The fact that the lower-rupture-force peak remains apparent at short dwell times, whereas the at long dwell times it only appears during the competition, shows that our experimental setup is not flawed (e.g., due to multiple rupture events). Accordingly, we conclude that the free 8-UTR_WT ORN binds strongly at the specific binding sites but leaves the unspecific binding sites free at long dwell times.

DISCUSSION

Binding modes and related free energies

Using SMFS, we show that the interaction between the RNA binding protein *At*GRP8 and its RNA target sequence is governed by at least two different binding mechanisms. The first binding mode represents an unspecific association that gets established in a rather short time (τ_1) and is characterized by a limited tightness and nesting of the two binding partners, resulting in relatively low binding forces. The average interaction lifetime of <1 s at a reaction length of 0.28 nm suggests that this bound state has a relatively low binding energy and can dynamically dissociate again. The incomplete blocking of the unspecific binding mode by an excess of free ORN in the competition experiment suggests that the protein *At*GRP8 very likely has several of these weak interaction sites. Furthermore, it is possible that this site can act as a metastable transition state into a state of higher conformational stability and binding specificity (dwell time τ_3), which is characterized by an increased bond tightness and nesting. The other binding mode could be identified as a sequence-specific binding site, yielding considerably larger (dissociation) forces, a bond lifetime of ~200 s and a largely increased bond reaction length of 0.55 nm, indicating a considerable increase of the related binding energy.

To determine the associated free energies, $\Delta G^0 = RT\ln(K_D) = RT\ln(k_{off}/k_{on})$, we have to estimate the reaction on-rate constant k_{on}, which is accessible by conventional RNA bandshift experiments. Quantitative titration in RNA bandshift experiments (for molecular ensembles, no discrimination of subpopulations) yields an averaged equilibrium constant of dissociation, K_D, of 2×10^{-7} M (Fig. S3), where $k_{on} = k_{off,\,all}/K_D = 0.027\,s^{-1}/2 \times 10^{-7}\,M = 1.4 \times 10^5\,M^{-1}\,s^{-1}$ can be derived from the values in Table 1. This value compares very well with typical values for association rate constants, k_{on}, describing the interaction of smaller receptor-ligand complexes in the diffusion limit (43). This allows now a sound estimate of $K_D = k_{off}/k_{on}$ and hence of the associated binding energies for the identified subpopulations related to τ_1 and τ_3. Based on our AFM-SMFS k_{off} data (Table 1), we can deduce equilibrium constants and associated free energies of $K_D = 1.3 \times 10^{-5}$ M and $\Delta G^0 = -28$ kJ/mol for the unspecific state, and $K_D = 3.4 \times 10^{-8}$ M and $\Delta G^0 = -42$ kJ/mol for the specific state. This observation is of particular interest, since a recent investigation of the *At*GRP7-RNA interaction using fluorescence correlation spectroscopy (44) predicted changes of the RNA conformation upon complex formation. Unfolding and opening of an artificial hairpin

containing the target sequence were observed upon *At*GRP7 binding.

Energy landscape of the interaction

Based on the above discussion, which makes use of the experimentally deduced reaction lengths, x_β, that are allocated to the different bound states, we propose a semiquantitative model of the possible binding energy landscape of this particular interaction (Fig. 6). Since the specific reaction length, x_β, represents the actual distance between the minimum of the binding potential and the position of the outermost transition state (the activation barrier) along the reaction coordinate, we can localize the first unspecific state at 0.28 nm behind the first activation barrier. From this metastable state, the complex can either dissociate or transform into the sequence-specific bound state, located 0.55 nm from the outer activation barrier. Due to its long biophysical lifetime of ~200 s, its binding affinity, K_D, and its related binding energy, ΔG^0, this state is assumed to be responsible for *At*GRP8 binding to its own RNA.

In summary, we demonstrate that AFM-based SMFS in combination with enhanced statistical data analysis techniques allows for discrimination, categorization, and quantification of complex interactions of biomolecules like binding of RBPs to their target sequences. For the chosen *At*GRP8 protein-RNA system, we found two different bound states, which differ in binding specificity, tightness, and affinity. The estimated binding free energies and the measured reaction lengths support a model where the specific and functional binding is introduced by a fast, unspecific, and metastable onset state. We propose that SMFS is a potent tool to dissect complex biomolecular interactions. The high sensitivity without the drawback of ensemble averaging should allow application of this method to the investigation of multivalent interactions.

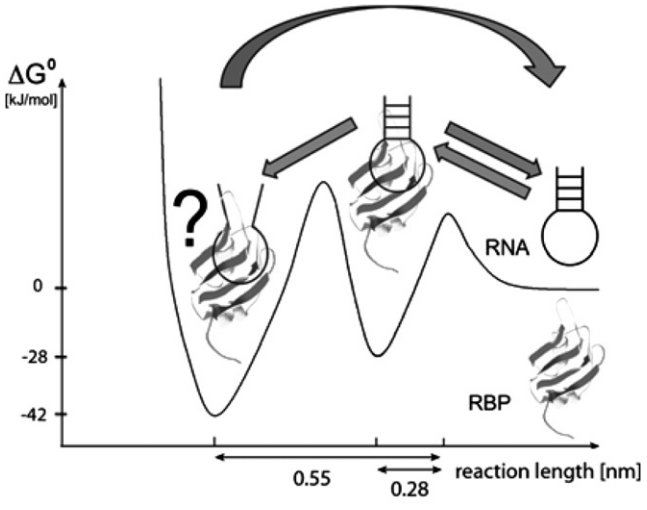

FIGURE 6 Schematic view of the proposed energy landscape and molecular binding mechanisms between 8-UTR_WT-SH ORN and *At*GRP8 according to our experimental single-molecule AFM results.

SUPPORTING MATERIAL

Three figures are available at http://www.biophysj.org/biophysj/supplemental/S0006-3495(09)00762-0.

We thank E. Detring for expert technical assistance and Sebastian Getfert and Peter Reimann for helpful discussions.

This work was supported by the Deutsche Forschungsgemeinschaft (SFB 613 and STA 653/2). J.C.S. is a fellow of the German National Academic Foundation.

REFERENCES

1. Moore, M. J. 2005. From birth to death: the complex lives of eukaryotic mRNAs. *Science*. 309:1514–1548.
2. Lorkovic, Z. J., and A. Barta. 2002. Genome analysis: RNA recognition motif (RRM) and K homology (KH) domain RNA-binding proteins from the flowering plant *Arabidopsis thaliana*. *Nucleic Acids Res.* 30:623–635.
3. Maris, C., C. Dominguez, and F. H. Allain. 2005. The RNA recognition motif, a plastic RNA-binding platform to regulate post-transcriptional gene expression. *FEBS J.* 272:2118–2131.
4. Hall, K. B. 2002. RNA-protein interactions. *Curr. Opin. Struct. Biol.* 12:283–288.
5. Schöning, J. C., C. Streitner, D. R. Page, S. Hennig, K. Uchida, et al. 2007. Autoregulation of the circadian slave oscillator component *At*GRP7 and regulation of its targets is impaired by a single RNA recognition motif point mutation. *Plant J.* 52:1119–1130.
6. Heintzen, C., M. Nater, K. Apel, and D. Staiger. 1997. *At*GRP7, a nuclear RNA-binding protein as a component of a circadian-regulated negative feedback loop in *Arabidopsis thaliana*. *Proc. Natl. Acad. Sci. USA*. 94:8515–8520.
7. Schöning, J. C., C. Streitner, I. M. Meyer, Y. Gao, and D. Staiger. 2008. Reciprocal regulation of glycine-rich RNA-binding proteins via an interlocked feedback loop coupling alternative splicing to nonsense-mediated decay in *Arabidopsis*. *Nucleic Acids Res.* 36:6977–6987.
8. Fu, Z. Q., M. Guo, B. R. Jeong, F. Tian, T. E. Elthon, et al. 2007. A type III effector ADP-ribosylates RNA-binding proteins and quells plant immunity. *Nature*. 447:284–288.
9. Streitner, C., S. Danisman, F. Wehrle, J. C. Schöning, J. R. Alfano, et al. 2008. The small glycine-rich RNA-binding protein *At*GRP7 promotes floral transition in *Arabidopsis thaliana*. *Plant J.* 56:239–250.
10. Bartels, F. W., M. McIntosh, A. Fuhrmann, C. Metzendorf, P. Plattner, et al. 2007. Effector-stimulated single molecule protein-DNA interactions of a quorum-sensing system in *Sinorhizobium meliloti*. *Biophys. J.* 92:4391–4400.
11. Bustamante, C., J. C. Macosko, and G. J. Wuite. 2000. Grabbing the cat by the tail: manipulating molecules one by one. *Nat. Rev. Mol. Cell. Biol.* 1:130–136.
12. Hinterdorfer, P., and Y. F. Dufrene. 2006. Detection and localization of single molecular recognition events using atomic force microscopy. *Nat. Methods*. 3:347–355.
13. Eckel, R., S. D. Wilking, A. Becker, N. Sewald, R. Ros, et al. 2005. Single-molecule experiments in synthetic biology: an approach to the affinity ranking of DNA-binding peptides. *Angew. Chem. Int. Ed. Engl.* 44:3921–3924.
14. Florin, E. L., V. T. Moy, and H. E. Gaub. 1994. Adhesion forces between individual ligand-receptor pairs. *Science*. 64:415–417.
15. Lee, G. U., L. A. Chrisey, and R. J. Colton. 1994. Direct measurement of the forces between complementary strands of DNA. *Science*. 266:771–773.

16. Hinterdorfer, P., W. Baumgartner, H. J. Gruber, K. Schilcher, and H. Schindler. 1996. Detection and localization of individual antibody-antigen recognition events by atomic force microscopy. *Proc. Natl. Acad. Sci. USA*. 93:3477–3481.

17. Dammer, U., M. Hegner, D. Anselmetti, P. Wagner, M. Dreier, et al. 1996. Specific antigen/antibody interactions measured by force microscopy. *Biophys. J.* 70:2437–2441.

18. Ros, R., F. Schwesinger, D. Anselmetti, M. Kubon, R. Schafer, et al. 1998. Antigen binding forces of individually addressed single-chain Fv antibody molecules. *Proc. Natl. Acad. Sci. USA*. 95:7402–7405.

19. Schwesinger, F., R. Ros, T. Strunz, D. Anselmetti, H. J. Guntherodt, et al. 2000. Unbinding forces of single antibody-antigen complexes correlate with their thermal dissociation rates. *Proc. Natl. Acad. Sci. USA*. 97:9972–9977.

20. Bartels, F. W., B. Baumgarth, D. Anselmetti, R. Ros, and A. Becker. 2003. Specific binding of the regulatory protein ExpG to promoter regions of the galactoglucan biosynthesis gene cluster of *Sinorhizobium meliloti*: a combined molecular biology and force spectroscopy investigation. *J. Struct. Biol.* 143:145–152.

21. Kuhner, F., L. T. Costa, P. M. Bisch, S. Thalhammer, W. M. Heckl, et al. 2004. LexA-DNA bond strength by single molecule force spectroscopy. *Biophys. J.* 87:2683–2690.

22. Eckel, R., R. Ros, B. Decker, J. Mattay, and D. Anselmetti. 2005. Supramolecular chemistry at the single-molecule level. *Angew. Chem. Int. Ed. Engl.* 44:484–488.

23. Neuert, G., C. Albrecht, E. Pamir, and H. E. Gaub. 2006. Dynamic force spectroscopy of the digoxigenin-antibody complex. *FEBS Lett.* 580:505–509.

24. Sulchek, T. A., R. W. Friddle, K. Langry, E. Y. Lau, H. Albrecht, et al. 2005. Dynamic force spectroscopy of parallel individual Mucin1-antibody bonds. *Proc. Natl. Acad. Sci. USA*. 102:16638–16643.

25. Bonanni, B., A. S. Kamruzzahan, A. R. Bizzarri, C. Rankl, H. J. Gruber, et al. 2005. Single molecule recognition between cytochrome *C* 551 and gold-immobilized azurin by force spectroscopy. *Biophys. J.* 89:2783–2791.

26. Henn, A., O. Medalia, S. P. Shi, M. Steinberg, F. Franceschi, et al. 2001. Visualization of unwinding activity of duplex RNA by DbpA, a DEAD box helicase, at single-molecule resolution by atomic force microscopy. *Proc. Natl. Acad. Sci. USA*. 98:5007–5012.

27. Bonin, M., J. Oberstrass, U. Vogt, M. Wassenegger, and W. Nellen. 2001. Binding of IRE-BP to its cognate RNA sequence: SFM studies on a universal RNA backbone for the analysis of RNA-protein interaction. *Biol. Chem.* 382:1157–1162.

28. Klaue, Y., A. M. Kallman, M. Bonin, W. Nellen, and M. Ohman. 2003. Biochemical analysis and scanning force microscopy reveal productive and nonproductive ADAR2 binding to RNA substrates. *RNA*. 9: 839–846.

29. Cho, Y., and A. Ivanisevic. 2006. Mapping the interaction forces between TAR RNA and TAT peptides on GaAs surfaces using chemical force microscopy. *Langmuir*. 22:1768–1774.

30. Vilfan, I. D., W. Kamping, M. van den Hout, A. Candelli, S. Hage, et al. 2007. An RNA toolbox for single-molecule force spectroscopy studies. *Nucleic Acids Res.* 35:6625–6639.

31. Evans, E., and K. Ritchie. 1997. Dynamic strength of molecular adhesion bonds. *Biophys. J.* 72:1541–1555.

32. Raible, M., M. Evstigneev, F. W. Bartels, R. Eckel, M. Nguyen-Duong, et al. 2006. Theoretical analysis of single-molecule force spectroscopy experiments: heterogeneity of chemical bonds. *Biophys. J.* 90:3851–3864.

33. Fuhrmann, A., S. Getfert, D. Anselmetti, P. Reimann, and R. Ros. 2008. Refined procedure of evaluating experimental single-molecule force spectroscopy data. *Phys. Rev. E.* 77:1–10.

34. Schöning, J. C., and D. Staiger. 2009. RNA-protein interaction mediating post-transcriptional regulation in the circadian system. *Methods Mol. Biol.* 479:337–351.

35. Staiger, D., L. Zecca, D. A. Wieczorek Kirk, K. Apel, and L. Eckstein. 2003. The circadian clock regulated RNA-binding protein *At*GRP7 autoregulates its expression by influencing alternative splicing of its own pre-mRNA. *Plant J.* 33:361–371.

36. Hutter, J. L., and J. Bechhoefer. 1993. Calibration of atomic-force microscope tips. *Rev. Sci. Instrum.* 7:1868–1873.

37. Ray, C., J. R. Brown, and B. B. Akhremitchev. 2007. Correction of systematic errors in single-molecule force spectroscopy with polymeric tethers by atomic force microscopy. *J. Phys. Chem. B.* 111:1963–1974.

38. Rief, M., F. Oesterhelt, B. Heymann, and H. E. Gaub. 1997. Single molecule force spectroscopy on polysaccharides by atomic force microscopy. *Science*. 275:1295–1297.

39. Evstigneev, M., and P. Reimann. 2003. Dynamic force spectroscopy: optimized data analysis. *Phys. Rev.* 68:045103.

40. Raible, M., M. Evstigneev, P. Reimann, F. W. Bartels, and R. Ros. 2004. Theoretical analysis of dynamic force spectroscopy experiments on ligand-receptor complexes. *J. Biotechnol.* 112:13–23.

41. Bell, G. I. 1978. Models for the specific adhesion of cells to cells. *Science*. 200:618–627.

42. Hartmann, R. K., A. Bindereif, A. Schön, and E. Westhof. 2005. Handbook of RNA Biochemistry. Wiley-VCH, Weinheim, Germany.

43. Schlosshauer, M., and D. Baker. 2004. Realistic protein-protein association rates from a simple diffusional model neglecting long-range interactions, free energy barriers, and landscape ruggedness. *Protein Sci.* 13:1660–1669.

44. Schüttpelz, M., J. C. Schöning, S. Doose, H. Neuweiler, E. Peters, et al. 2008. Changes of conformational dynamics of mRNA upon *At*GRP7 binding studied by fluorescence correlation spectroscopy. *J. Am. Chem. Soc.* 30:9507–9513.